Supplement of Atmos. Chem. Phys., 21, 1325–1340, 2021
https://doi.org/10.5194/acp-21-1325-2021-supplement

Atmospheric Chemistry and Physics
Open Access
EGU

Supplement of

Ozonolysis of fatty acid monolayers at the air–water interface: organic films may persist at the surface of atmospheric aerosols

Benjamin Woden et al.

Correspondence to: Christian Pfrang (c.pfrang@bham.ac.uk)

Electronic Supplementary Information

Section S1 – Monolayer Characterisation at Low Temperature

In order to ensure that the system could effectively be modelled as a monolayer for neutron reflectometry data fitting, and to find an optimum spreading volume that packs in a similar manner across the temperature ranges studied (to ensure that temperature effects alone, rather than effects due to monolayer phase, were studied), monolayers of oleic acid were spread on pure water and 0.6 M NaCl solution subphases at room temperature, just above and just below ice melting point (not accessible for pure water) and Wilhelmy tensiometric measurements were performed using a Langmuir trough equipped with a NIMA surface pressure sensor and control software. π-A isotherms were recorded and are shown below in Figures S1 and S2.

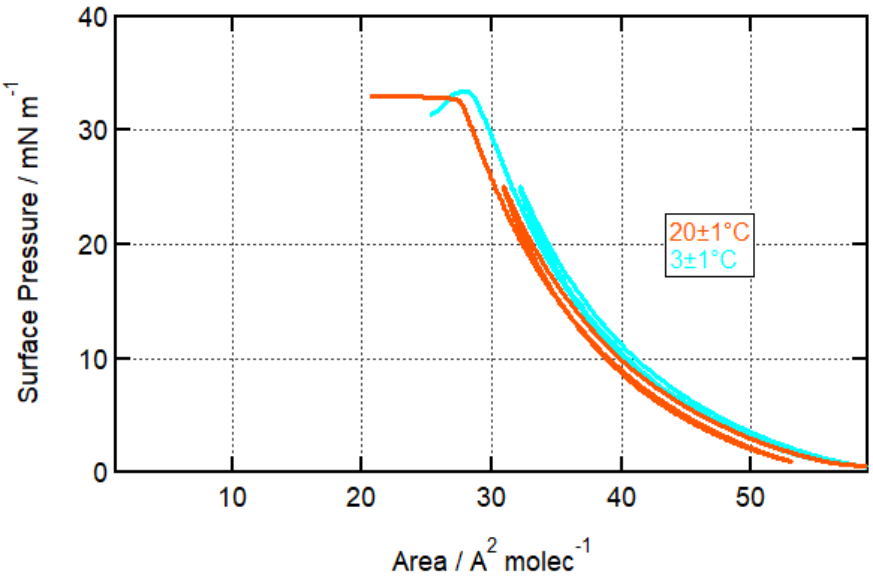

Figure S1: π-A Isotherm for oleic acid on pure water at 3 °C (aqua) and 20 °C (orange).

These tensiometry experiments showed that the system could be described as a well-behaved monolayer over the temperature range of interest on pure water and NaCl solution.

The impact of temperature on the π-A isotherm for oleic acid was not large, and indeed was not reliably distinguishable from zero by our apparatus and method. Due to this, the target surface area per molecule of 30 Å^2 used for previous experiments at room temperature was deemed suitable for use at the lower temperature as well. This choice of initial surface concentration

maximises initial signal for neutron reflectometry and infrared spectroscopy measurements without risking film breakage.

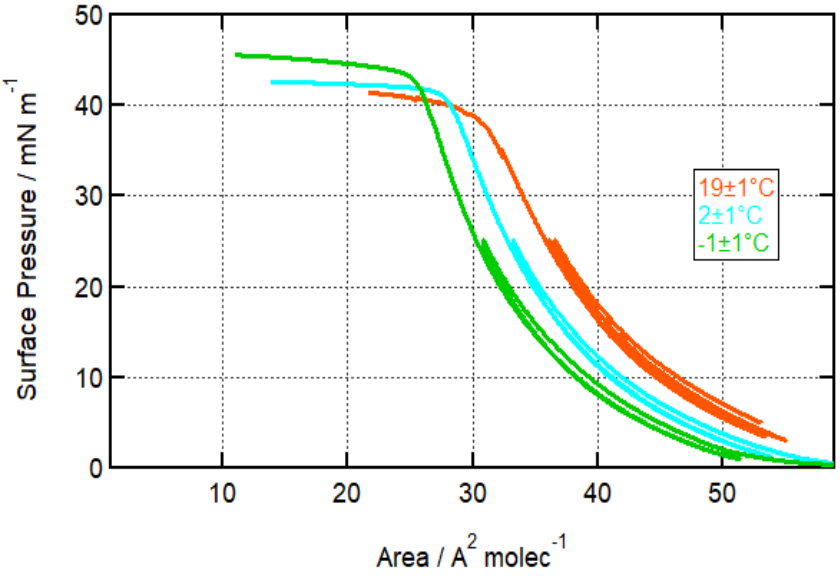

Figure S2: π-A Isotherm for oleic acid on 36 g L^{-1} NaCl at -1 °C (green), 2 °C (aqua) and 19 °C (orange).

The situation on the NaCl solution subphase was somewhat different. Compared with the pure water condition, significantly higher surface pressure regimes are accessible before the breaking of the monolayer at all temperatures and these are associated in the low temperature conditions with slightly higher surface concentrations. There is an observable trend of lower surface pressure with lower temperature at a given surface concentration, and this trend does not appear to be linear. These results are consistent with earlier findings by Knopf and Forrester (2011).

Based on these results, the target surface area per molecule of 30 $Å^2$ used for the pure water condition was extended to the NaCl solution condition at all temperatures. Preserving consistency across conditions and maximising observable signal were considered highly important, and the slight risk of overspreading in the room temperature NaCl solution condition (which was not observed during experiments) was deemed acceptable to achieve this, particularly as preliminary neutron reflectometry data gathered with an early prototype of the apparatus (ISIS INTER reflectometer; RB 1710483) had suggested that this was the least interesting of the new conditions under study.

Section S2 – Reflectivity Curves

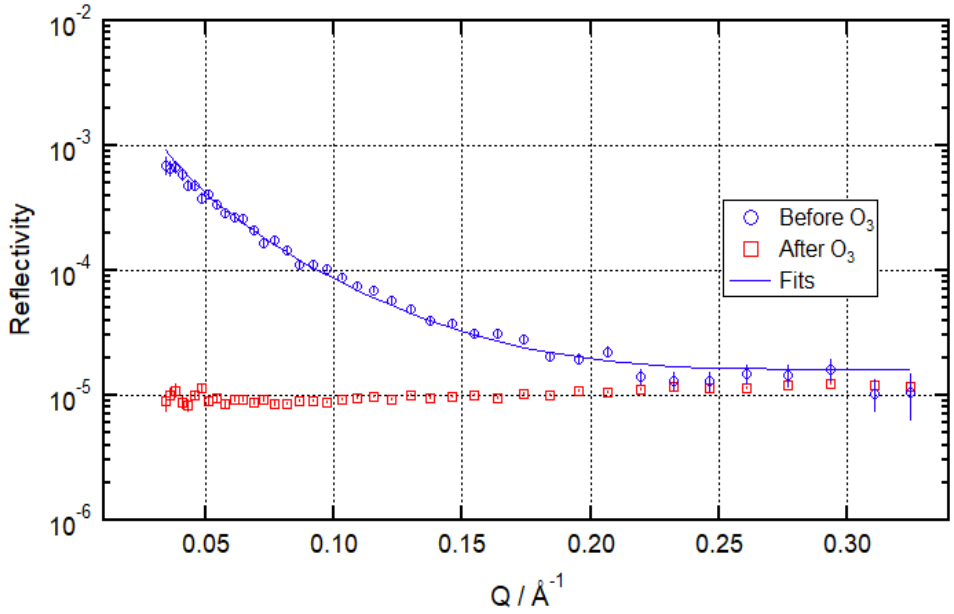

Figure S3: Reflectivity before ozonolysis (blue circles), and after ozonolysis (red squares) for ozonolysis of 29 µL 1.0 g L^{-1} d_{34}-OA ($CHCl_3$ spread. sol.) on pure water subphase by 323 ± 29 ppb O_3 introduced at t = 0 s at 21 ± 1 °C.

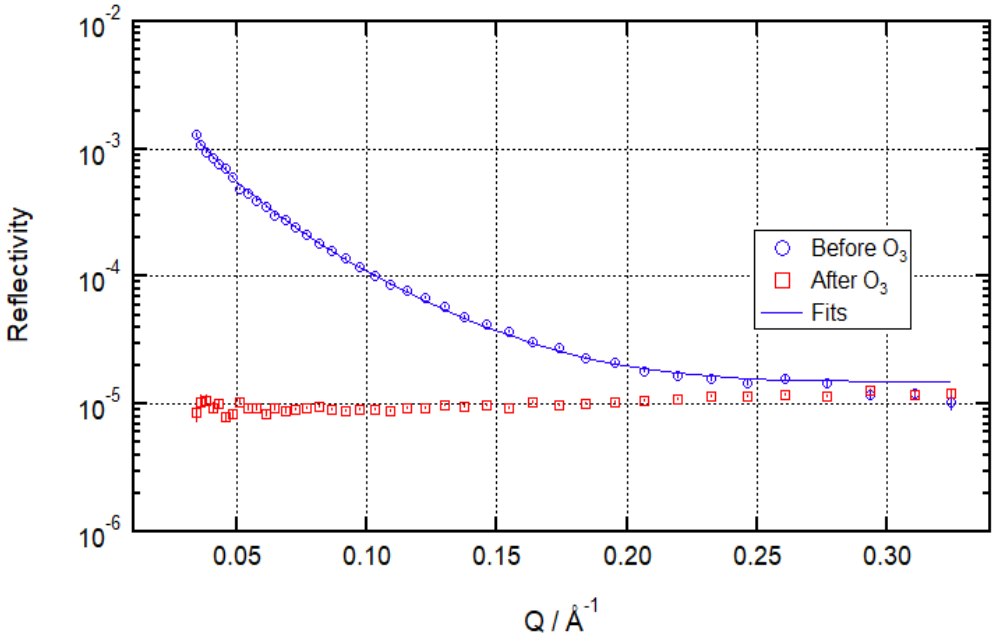

Figure S4: Reflectivity before ozonolysis (blue circles), and after ozonolysis (red squares) for ozonolysis of 25 µL 1.0 g L^{-1} d_{34}-OA ($CHCl_3$ spread. sol.) on 36 g L^{-1} NaCl(aq) subphase by 323 ± 29 ppb O_3 introduced at t = 0 s at 21 ± 1 °C.

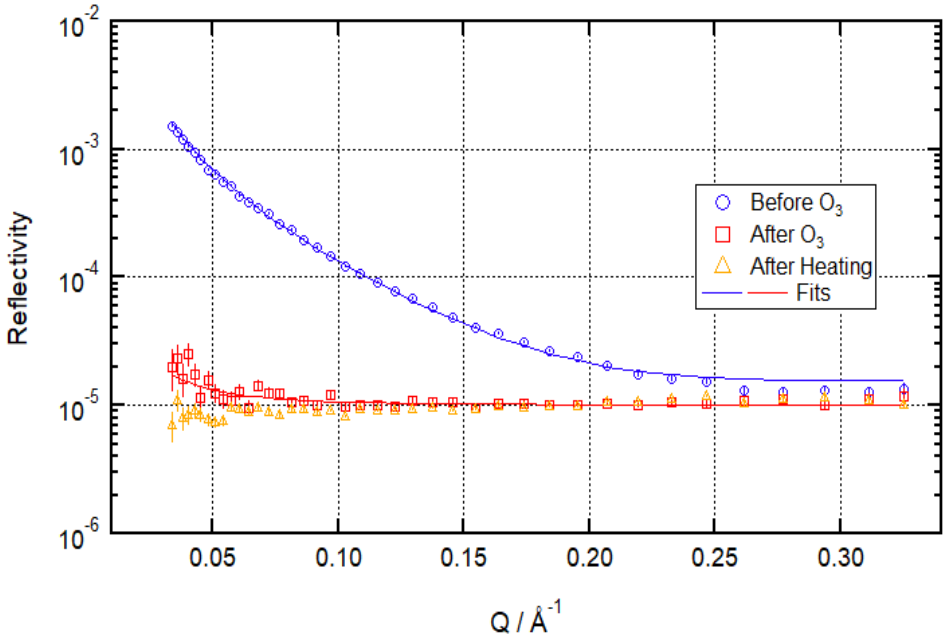

(a)

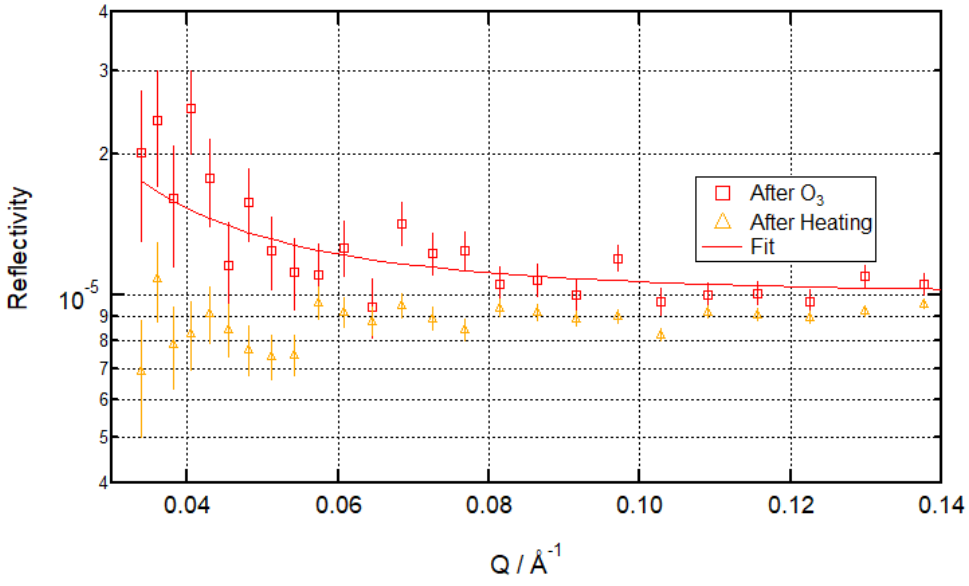

(b)

Figure S5: (a) Reflectivity before ozonolysis (blue circles), after ozonolysis (red squares) and after heating (orange triangles) for ozonolysis of 25 µL 1.0 g L^{-1} d_{34}-OA ($CHCl_3$ spread. sol.) on 36 g L^{-1} NaCl(aq) subphase by 323 ± 29 ppb O_3 introduced at t = 0 s at -2 ± 1 °C; (b) zoomed in Fig. S5(a) to illustrate the clear presence of a residue (red squares) that is lost upon heating (orange triangles).

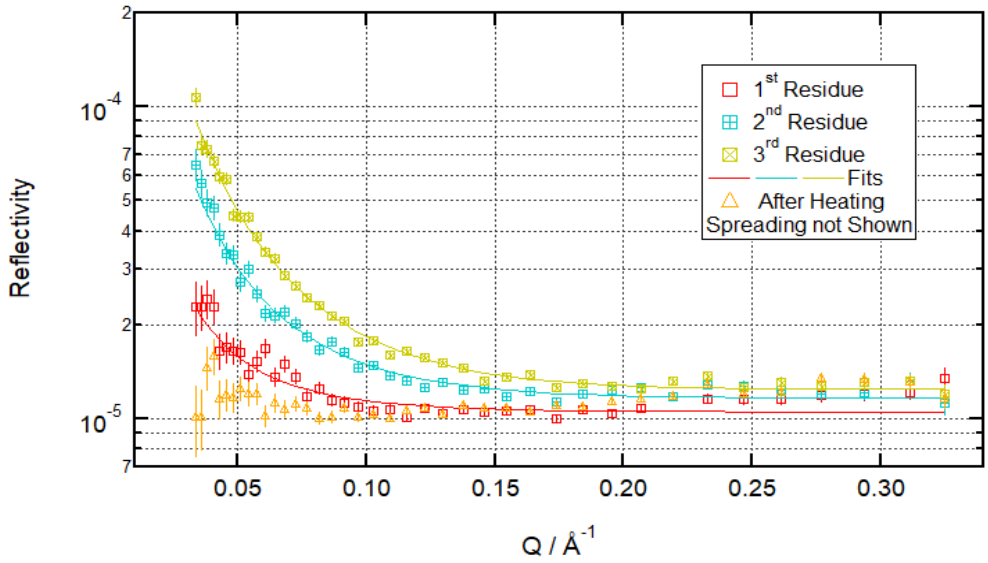

Figure S6: Reflectivity after ozonolysis from the first (open red squares), second (teal squares with an upright cross), and third (olive squares with a diagonal cross) ozonolysis steps, and after heating (orange triangles) for the multi-ozonolysis reaction shown in Figures 4 and 5 (main paper).

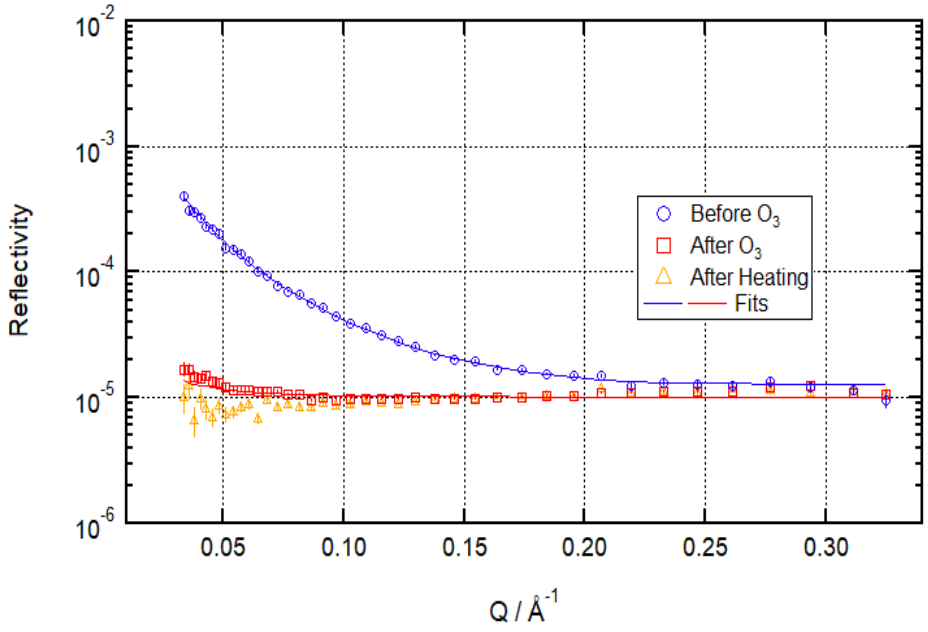

Figure S7: Reflectivity before ozonolysis (blue circles), after ozonolysis (red squares) and after heating (orange triangles) for ozonolysis of 17 µL 1.3 g L^{-1} d_{18}-OA ($CHCl_3$ spread. sol.) on pure water subphase by 323 ± 29 ppb O_3 added at t = 0 s at 3 ± 1 °C.

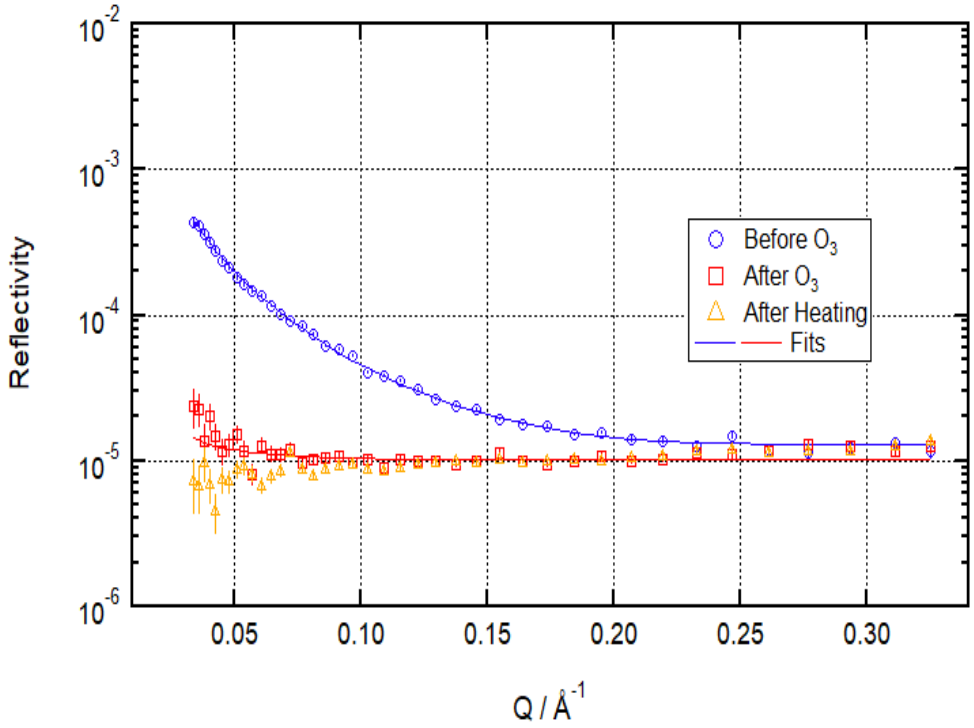

Figure S8: Reflectivity before O_3 (blue circles), after O_3 (red squares) and after heating (orange triangles) for ozonolysis of 17 µL 1.0 g L^{-1} d_{18}-OA ($CHCl_3$ spread. sol.) on 36 g L^{-1} NaCl(aq) subphase by 323 ± 29 ppb O_3 added at t = 0 s at -2 ± 1 °C.

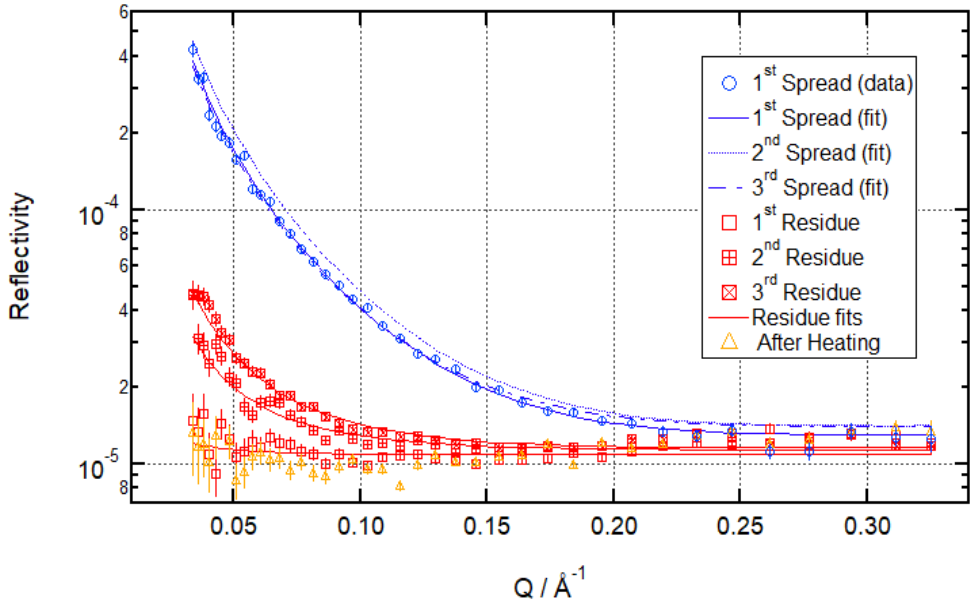

Figure S9: Reflectivity before ozonolysis (blue circles (data only shown for first spreading; fits shown for all three spreadings), after ozonolysis (red squares) and after heating (orange triangles) for a multi-ozonolysis reaction (analogous to that shown in Figures 4 and 5 (main paper) and S6) of 17 µL 1.0 g L^{-1} d_{18}-OA at 3 ± 1 °C.

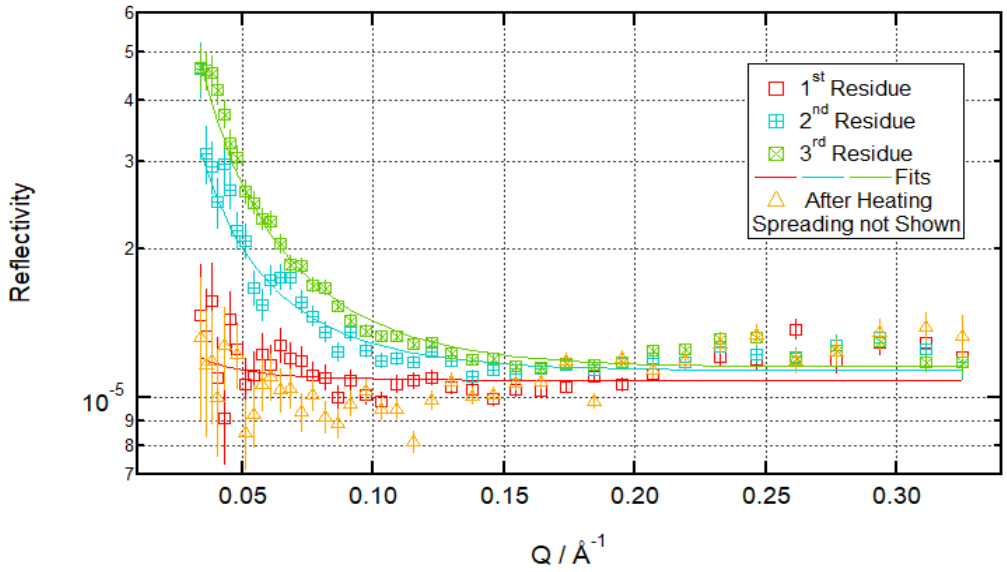

Figure S10: Reflectivity after ozonolysis from the first (open red squares), second (teal squares with an upright cross), and third (olive squares with a diagonal cross) ozonolysis steps, and after heating (orange triangles) for the multi-ozonolysis reaction shown in Figure S9.

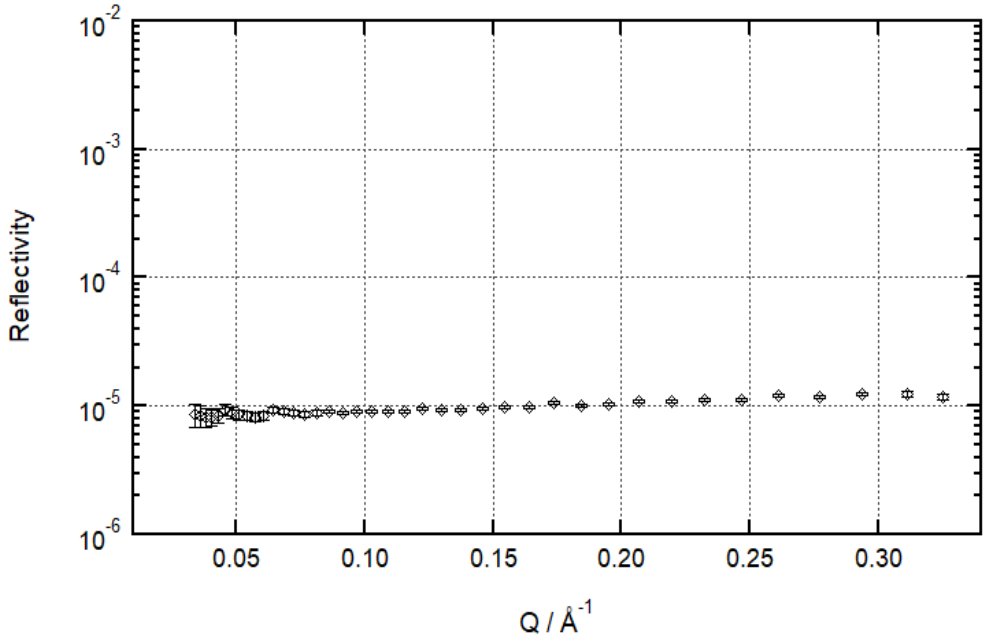

Figure S11: Reflectivity for a pure null-reflecting air–water interface.

Section S3 – Kinetic Fitting

In the latter stages of the reaction, reflectometry signal from products is likely to be a significant or even dominant contributor to reflectivity. Indeed, the primary case made in this paper is that we can use residual reflectivity that cannot be depressed by further ozonolysis at low temperatures to infer the presence of a residual monolayer of reaction products. As a result, we do not attempt to fit data for lower surface coverage values than 10^{14} cm^{-2} (as calculated by fitting reflectivity curves and assuming all reflectivity is due to oleic acid). This represents approximately the final third of the reaction in terms of reflectivity, and was chosen as it is at this point that significant deviations from a smooth, regular function are observed from a basic visual appraisal of the data. However, even before this point, some of the measured reflectivity will be due to the presence of reaction products at the interface (whether or not they are sufficiently stable to persist at the end of the reaction), meaning that calculations of oleic acid surface coverage will be over-estimations to some degree as soon as the reaction begins, and to a greater and greater extent as the reaction progresses. As a result, fitted pseudo-1st-order rate constants are likely to be slight under-estimations, even when the latter third of the reaction is excluded from the fitting.

Another complication involves the mixing of O_3 into the chamber at the very start of the reaction. The model presented in equation 1 assumes that $[O_3]_{gas}$ is uniform throughout the reaction chamber. This is, in reality, not the case. O_3 is introduced to the chamber through a long tube running down one size of the chamber just above the air/water interface with holes of varying diameters drilled along its length. This oxidant gas ingress system was designed by a previous member of this research group in order to achieve even distribution of the oxidant gas with respect to the long edge of the interface (it is unavoidably still the case that there is a concentration gradient across the short edge) and the precise sizes of the drilled holes were tuned in order to achieve even mixing based on fluid dynamics simulations (Sebastiani, 2014; Sebastiani et al., 2015). The mixing time for the cell is estimated as around 60 s. As a result of this, $[O_3]_{gas}$ will rise much more quickly in a boundary layer just above the air/water interface at around the height of the ingress pipe than it will in the chamber as a whole. It is, of course, the $[O_3]_{gas}$ just above the interface that is relevant for the progress of the reaction. This boundary layer constitutes an 'effective volume' for the reaction which is significantly lower than the total volume of the reaction chamber. Determining the volume of this boundary layer is not experimentally possible, and its value is unfortunately something of a fudge factor in fitting rate constants to these data. Assuming too high an effective volume will mean that the model underestimates the time it takes for the reaction to 'get up to speed', meaning that too high a rate constant will be fitted to compensate.

Usefully, this effect scales with $[O_3]_{gas}$. Choosing too high an effective volume (for instance by using the entire chamber volume of 2.1×10^3 cm^3) results in very poor fitting at higher values of $[O_3]_{gas}$, and causes fitted k_1 values to show a superlinear relationship with $[O_3]_{surf}$, meaning no 2nd-order rate constant can be determined. Choosing too low an effective volume results in very poor fitting at lower values of $[O_3]_{gas}$ and a sublinear relationship between k_1 and $[O_3]_{surf}$. It is possible, therefore, to estimate a boundary layer volume by appraising both the quality of fits between model and data at various values of $[O_3]_{surf}$, and by assessing the relationship between k_1 and $[O_3]_{surf}$, which should be linear (due to the 2nd-order nature of the reaction). As long as the same boundary layer is used, fitted parameters from different experiments will be meaningfully comparable.

For this work, a boundary layer volume of 35 cm^3 (or a boundary layer height above the interface of 2 mm) was used, as it was appraised to produce a reasonable quality of fit for experimental data across the range of $[O_3]_{gas}$ conditions studied, and produced suitably linear relationship between k_1 and $[O_3]_{surf}$ in order for a 2nd-order rate constant (k_2) to be calculated.

This is further complicated due to experimental uncertainty regarding the exact time of the start of the reaction. The reaction is started by manually uncovering part of the UV lamp inside the ozoniser, and the moment at which this action is performed is treated as t_0 for that reaction. However, this manual process is only as precise and reproducible as the finger movements required to perform it. Sometimes, the lamp might be uncovered more slowly than others. Sometimes, the sheath might stick slightly, delaying the uncovering of the lamp by a second or two. Sometimes, the experimenter might overshoot the desired sheath position, uncovering slightly more of the lamp than intended for a fraction of a second. The situation is yet further complicated by the fact that the 'head' of O_3 produced still has to travel a few metres down the tube before it enters the chamber.

When fitting this kind of exponential function, the first few points exercise a high degree of leverage over the whole fit. However, it is exactly these first few points (reflectivity data are collected in 5 second frames for these experiments) that suffer from this uncertainty over the precise start time of the reaction. In order to overcome this difficulty, the first three points (15 seconds) of each reaction are not fitted, and a time offset parameter is added to the model (each instance of "t" on the right-hand-side of equation 2 is replaced by a "$(t-t_{offset})$" term). This produces the problem that t_{offset} is somewhat correlated with Γ_0 – the reaction can be modelled to have started arbitrarily far back into the past before the fitted data as long as the starting surface coverage is raised to correspondingly high and physically unrealistic values. In order to avoid this, Γ_0 is measured before the reaction begins (under a stream of O_2 containing no O_3) and the parameter is fixed for each fitting based on this measurement. Fitting then proceeds by allowing k_1 and t_{offset} to vary, and fits are achieved by this method that tend to converge on values of t_{offset} (generally 10 – 20 s) that make physical sense.

Variation in the assumptions outlined above result in good agreement between model and data for each experiment and produce k_1 values that differ by as much as 15 % from the values produced via the fitting methods settled upon. This error (which is far greater than the error associated with reflectivity fitting at each individual point, and therefore dominates the error in fitted k_1 values) is reflected in our final calculated values for the 2nd-order rate constant.

This error due to model subjectivity turned out to have a much greater effect on the robustness of the fitted k_1 values than did the first problem discussed here (that of deciding what portion of the end of the reaction to discard from fitting due to overbearing influence on fitted surface coverage values of reflectivity due to reaction products). The choice of where to stop fitting made much less difference to the resultant fit than did the choice of where to start fitting and what boundary layer volume to use.

This analytical fitting process does involve the piling of several epicycles upon the basic model of a 2nd-order reaction in which one component in excess, producing a series of pseudo-1st-order reactions with rate constants proportional to the concentration of the excess component. Particularly with regard to the $[O_3]_{gas}$ gradient at the start of the reaction, these epicycles are somewhat arbitrary and depend on human judgement in terms of assessing linearity of the 2nd-order plot and goodness of fit

of the 1st-order plots. The problem could be avoided by using a numerical model to explicitly represent the surface concentrations of oleic acid and all likely deuterated products and intermediates and the rates at which those products and intermediates are produced, decay, and partition away from the surface into the bulk phase or gas phase, as well as to explicitly represent the spatial and temporal gradients of $[O_3]_{gas}$ within the chamber. Several numerical models focusing on the first part of this (explicitly dealing with various transient species and products at the interface, as well as in multiple layers) are under development by this research group in collaboration with others, and their use has already yielded significant contributions in the field of aerosol kinetics (Pfrang et al., 2010, 2011; Sebastiani et al., 2018; Shiraiwa et al., 2010, 2012).

However, a full investigation of the detailed kinetics of this reaction is considered out of scope for this study, as it has been studied before (King et al., 2009), and the primary purposes of this work is to investigate differences between the reaction at room temperature and at a more atmospherically realistic near-freezing temperature. As is made clear in the presentation of the results of this kinetic fitting in the main text, this simpler analytic approach demonstrates that there is not a significant difference in the kinetics of the reaction between these two temperature conditions. As a result, it was not considered worthwhile to deploy the numerical model in order to attempt to account for the slight systematic bias towards underestimation of rate constants present in the analytical model, as it would be exceedingly unlikely to uncover anything of further interest.

Figure S12 shows an example of equation 2 fitted to a kinetic time series as described above.

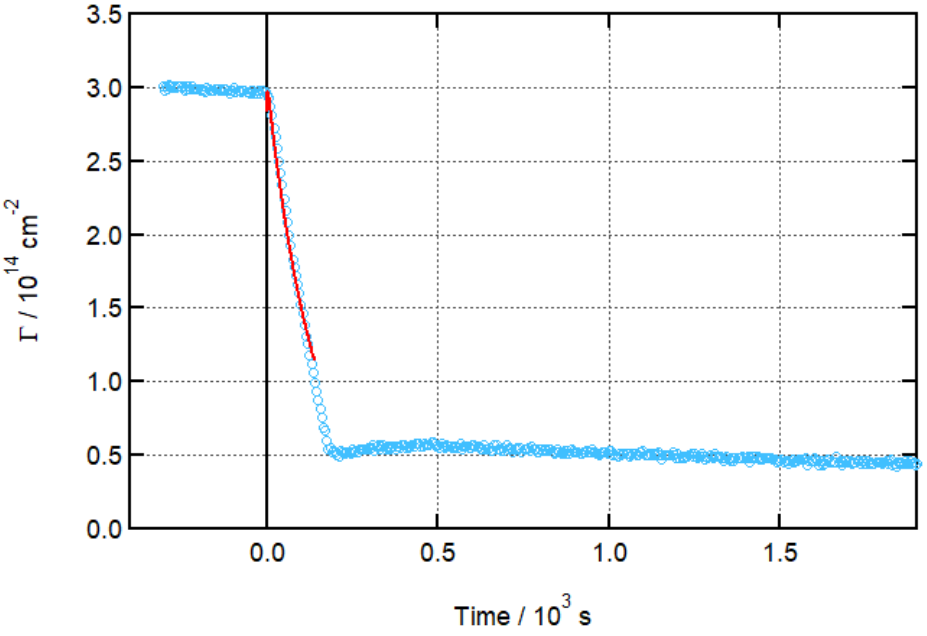

Figure S12: Time evolution plot for ozonolysis of 39 µL 0.75 g L^{-1} d_{34}-OA ($CHCl_3$ spread. sol.) on pure water subphase by 503 ± 60 ppb O_3 introduced at t = 0 s at 2 ± 1 °C showing Eq. (2) (main paper) fitted to the data; error bars omitted for visual clarity.

Section S4 – IRRAS Data

As mentioned in the method section, this work was carried out in a reaction chamber designed for the integration of simultaneous *in situ* IRRAS measurements on a neutron reflectometry beamline. This equipment was deployed and used for the experiments carried out on INTER, but could not be deployed on FIGARO due to space restrictions. IRRAS integration is primarily intended to facilitate the study of mixed monolayers, in which one component can be deuterated (for neutron reflectometry) and the other left non-deuterated (and thus easily measurable by IRRAS). As the work discussed here focused entirely on single-component monolayers, the IRRAS data did not provide any additional insight. IRRAS can also measure deuterated components (the IR absorbance bands are shifted to a lower wavenumber, distinguishing them from the absorbance bands associated with non-deuterated components), but the sensitivity in this region is much lower, as these bands are weaker and more affected by atmospheric interference. This means that IRRAS measurements cannot distinguish the residues left at low temperatures from background noise. Figure S13 shows an example of IRRAS data from an ozonolysis experiment on INTER.

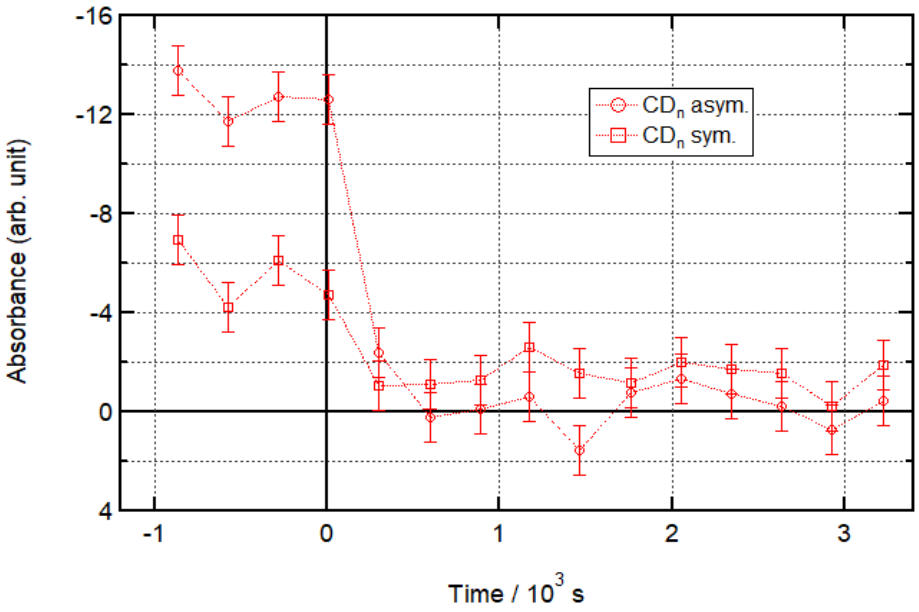

Figure S13: Time evolution plot for ozonolysis of 29 µL 1.0 g L^{-1} d_{34}-OA ($CHCl_3$ spread. sol.) on pure subphase by 323 ± 29 ppb O_3 introduced at t = 0 s at 21 ± 1 °C showing integrated IR absorbance for CD_n asymmetric (circles) and symmetric (squares) bands.

Section S5 – Stability Run

In order to ensure that the monolayer was stable at low temperatures, and that the reactions observed were chemical oxidation on the introduction of O_3, and not confounded by significant loss of material through physical or chemical processes unrelated to ozonolysis, a long exposure of an oleic acid to a pure O_2 flow was performed, and the results are shown in Figure S14 below.

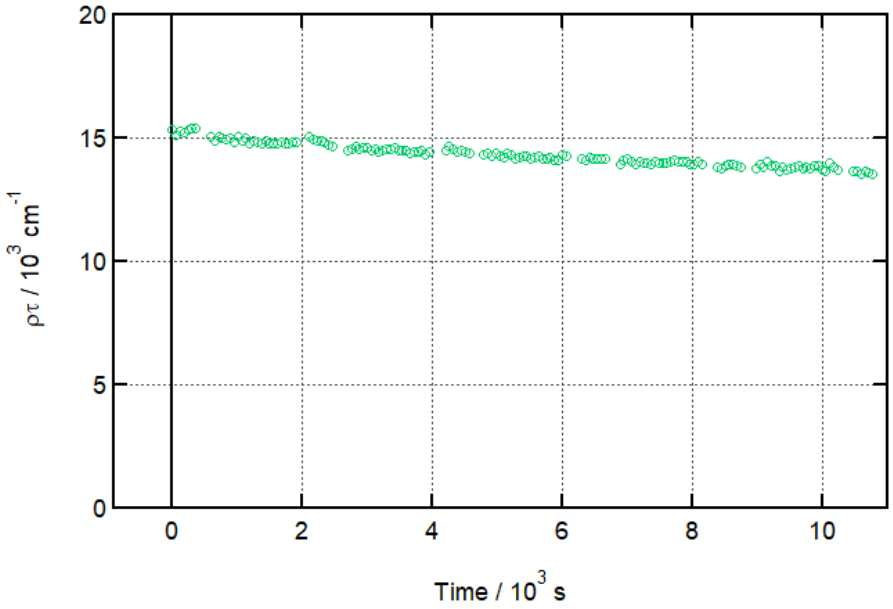

Figure S14: Stability run; time evolution plot for 30 µL 1.2 g L^{-1} d_{34}-OA ($CHCl_3$ spread. sol.) at 3 ± 2 °C on pure water subphase under pure O_2 flow; error bars omitted for visual clarity. ρτ is the product of neutron scattering length density and layer thickness is it proportional to the surface excess $\Gamma = \frac{\tau\rho}{b}$, where b is the scattering length of the molecule (d_{34}-OA).

References

King, M. D., Rennie, A. R., Thompson, K. C., Fisher, F. N., Dong, C. C., Thomas, R. K., Pfrang, C. and Hughes, A. V.: Oxidation of oleic acid at the air-water interface and its potential effects on cloud critical supersaturations., Phys. Chem. Chem. Phys. , 11(35), 7699–7707, doi:10.1039/b906517b, 2009.

Knopf, D. A., and S. M. Forrester, Freezing of Water and Aqueous NaCl Droplets Coated by Organic Monolayers as a Function of Surfactant Properties and Water Activity, J. Phys. Chem. A, 115(22), 5579–5591, 2011.

Pfrang, C., Shiraiwa, M. and Pöschl, U.: Coupling aerosol surface and bulk chemistry with a kinetic double layer model (K2-SUB): oxidation of oleic acid by ozone, Atmos. Chem. Phys., 10(10), 4537–4557, doi:https://doi.org/10.5194/acp-10-4537-2010, 2010.

Pfrang, C., Shiraiwa, M. and Poschl, U.: Chemical ageing and transformation of diffusivity in semi-solid multi-component organic aerosol particles, Atmos. Chem. Phys., 11(14), 7343–7354, doi:10.5194/acp-11-7343-2011, 2011.

Sebastiani, F.: Neutron reflectometry and Ellipsometry applied to ATmospheric Night-time Oxidation, University of Reading, PhD thesis, 2014.

Sebastiani, F., Campbell, R. A. and Pfrang, C.: Complementarity of neutron reflectometry and ellipsometry for the study of atmospheric reactions at the air–water interface, RSC Adv., 5(129), 107105–107111, doi:10.1039/C5RA22725A, 2015.

Sebastiani, F., Campbell, R. A., Rastogi, K. and Pfrang, C.: Night-time oxidation of surfactants at the air–water interface: effects of chain length, head group and saturation, Atmos. Chem. Phys., 18, 3249–3268, 2018.

Shiraiwa, M., Pfrang, C. and Pöschl, U.: Kinetic multi-layer model of aerosol surface and bulk chemistry (KM-SUB): the influence of interfacial transport and bulk diffusion on the oxidation of oleic acid by ozone, Atmos. Chem. Phys., 10(8), 3673–3691, doi:https://doi.org/10.5194/acp-10-3673-2010, 2010.

Shiraiwa, M., Pfrang, C., Koop, T. and Pöschl, U.: Kinetic multi-layer model of gas-particle interactions in aerosols and clouds (KM-GAP): linking condensation, evaporation and chemical reactions of organics, oxidants and water, Atmos. Chem. Phys., 12(5), 2777–2794, doi:https://doi.org/10.5194/acp-12-2777-2012, 2012.